HOOC-EM: Fast Beam Sweeping for LEO Mega-Constellation Customer Terminals

Samuel C. Morgan and Todd E. Humphreys
Department of Aerospace Engineering and Engineering Mechanics, The University of Texas at Austin

BIOGRAPHIES

Samuel C. Morgan (B.S.E., Murray State University; M.S., Auburn University) is a P.h.D. student in the department of Aerospace Engineering and Engineering Mechanics at The University of Texas at Austin, and a member of the UT Radionavigation Laboratory. His research interests include fused LEO GNSS and signal processing.

Todd E. Humphreys (B.S., M.S., Utah State University; Ph.D., Cornell University) holds the Ashley H. Priddy Centennial Professorship in Engineering in the Department of Aerospace Engineering and Engineering Mechanics at The University of Texas at Austin. He is Director of the Wireless Networking and Communications Group and of the UT Radionavigation Laboratory, where he specializes in the application of optimal detection and estimation techniques to positioning, navigation, and timing. His awards include the UT Regents' Outstanding Teaching Award (2012), the NSF CAREER Award (2015), the ION Thurlow Award (2015), the PECASE (NSF, 2019), and the ION Kepler Award (2023). He is Fellow of the Institute of Navigation and of the Royal Institute of Navigation.

ABSTRACT

The popularity of low Earth orbit (LEO) satellite broadband networks has grown significantly in the past decade. These LEO networks transmit at high carrier frequencies due to spectral availability, resulting in narrow beamforming at the satellite and customer terminal (CT). However, existing methods for beam sweeping have only been developed for terrestrial mmWave networks (e.g., IEEE 802.11ad, IEEE 802.11ay, IEEE 802.15.3c, and the 3GPP's 5G NR). These standards call for exhaustive beam sweeping procedures, selecting the best candidate beam pair after each azimuth and elevation is searched. Such methods are unsuitable for LEO network CTs due to satellite dynamics and frequent satellite handoff. This paper proposes a maximum likelihood (ML) technique for CT beam sweeping in LEO broadband networks. The proposed method, called hexagonal odds-based orbital comb and entrainment method (HOOC-EM), first divides the celestial sphere into hexagonal and pentagonal sectors, according to CT beamwidth. A probability density function (PDF) is applied to the sectors and each sector is searched in a ML fashion (i.e., the most likely sector is searched first and so on) stopping once a signal is detected. An empirical *a priori* PDF and a Markov model are developed using orbital simulations of the constellation. The *a priori* PDF is dynamically updated according to the Markov model to account for satellite dynamics. This paper compares HOOC-EM to other ML methods informed by two other *a priori* PDFs, one uniform, and one linear with respect to elevation. These latter methods are not updated dynamically according to the Markov model. HOOC-EM is also compared to a traditional exhaustive raster scan beam sweep. The performance of the proposed method is analyzed by comparing the average time to detection as a function of receiver beamwidth. Numerical results indicate that HOOC-EM is an effective method for LEO broadband beam sweeping and superior to other techniques in cases where the Markov model is recent.

I. INTRODUCTION

High data throughput has rapidly become a necessity, enabling high-quality video streaming, efficient remote work, and realistic, low-latency extended and/or augmented reality experiences, among other applications. To meet the growing demand, broadband network providers have sought to increase data throughput. Achieving high data throughput requires changes to the physical (PHY) layer, particularly in terms of the bandwidth of the transmitted radio frequency (RF) signal, which is directly related to the maximum data rate. Therefore, a wide bandwidth is required to enable high data throughput. To avoid in-band interference, sufficient spectral availability at the transmitted center frequency is necessary.

Lower center frequencies are often desirable because they are less susceptible to attenuation and experience less free space path loss. However, there is limited spectral availability at lower frequencies, leading to the recent popularity of transmitting at a higher center frequencies (e.g., mmWave), where there is ample available spectrum [Rappaport et al., 2014]. The downside to higher frequencies is the much lower received signal power due to attenuation and path loss. To mitigate these downsides, beamforming at both transceivers (TX/RX) is used. Beamforming allows for high frequency signals to be received at adequate power levels by focusing all the TX/RX gain in a narrow beam in a specific direction. However, this does add a spatial component to network access, complicating sustained base station (BS) and customer terminal (CT) communication and CT

Preprint of the 2024 ION GNSS+ Conference Baltimore, MD, Sep. 16-20, 2024

network entry [Andrews et al., 2014].

Wireless communications networks prescribe various protocols for the CT to enter the network. Network entry is defined as the CT being able to send and receive data as a fully integrated node. This implies that the network, including the CT, knows enough about the location of the CT, and time and frequency offsets, to engage in the resource allocation scheme the network uses to coordinate traffic (e.g., time and/or frequency division duplexing). The first step in resolving these unknowns and ultimately entering the network in all existing mmWave standards is beam sweeping. Beam sweeping aims to align the beams of the transmitter and receiver. In terrestrial networks this involves the receiver and/or transmitter sweeping all feasible directions using a predefined codebook [Xue et al., 2024].

In three of the IEEE's mmWave standards (i.e., IEEE 802.11ad, IEEE 802.11ay, and IEEE 802.15.3c) a two-stage beam sweeping procedure is employed, beginning with what is called a sector-level sweep (SLS) [Nitsche et al., 2014, Ghasempour et al., 2017, Baykas et al., 2011]. In the SLS large, low-resolution beams are used to search all directions in the codebook of the CT. Once all sectors are searched, the highest power sector is then searched using a narrow, high-resolution beam, and the optimal beam pair is selected. It is worth noting that both the transmitter and receiver must perform beam sweeping and take on the roles of initiator and responder to establish a beam pair. In the 3GPP's 5G NR standard, an exhaustive search is performed by the gNodeB and/or CT to determine the best beam pair by checking the reference signal received power and/or the signal-to-interference-plus-noise ratio (SINR) [Heng et al., 2021].

The standards discussed thus far were designed primarily for terrestrial networks, which are inherently limited by existing infrastructure. As a result, terrestrial networks often fail to provide adequate coverage in remote or rural areas. Non-terrestrial networks (NTNs) were introduced to address this issue by providing coverage anywhere on Earth by using satellites in low Earth orbit (LEO), medium Earth orbit (MEO), and geostationary orbit (GEO), together with high-altitude platforms (HAPS). In general, NTNs take two forms: direct to cell (D2C) or very short aperture terminals (VSATs). This paper focuses on NTNs that use VSATs (i.e., a CT is a VSAT). Among these, LEO satellite NTNs using VSATs are the most widespread, with SpaceX's Starlink being the most notable example.

The beam sweeping protocols discussed in the IEEE standards present obvious challenges if applied to a LEO broadband system. Due to satellite or CT dynamics, the best beam pair at the start of a search may no longer be the best at the end. Additionally, the distance between the satellite and CT may make it difficult for any given CT to participate in the two-way initiator-responder pairing technique. Furthermore, technical issues arise when devices equipped to use the current standards experience Doppler shifts and time delays that would ordinarily be impossible for terrestrial networks, even with high CT dynamics.

The 3GPP began studying NTNs for use with 5G NR as early as Release 15 [3GPP, 2017]. They begin discussing beam management in Release 16, with a primary focus on the satellite side [3GPP, 2023]. To date, no final decisions have been made on how to handle beam management in NTN in NR and 6G, so the basic terrestrial framework developed in Release 15 is used as a baseline. Some researchers have made suggestions to improve beam management in NR NTNs [Rinaldi et al., 2020, Kim et al., 2020, Wei et al., 2023], while some test the current standard. For instance, [Artiga and Vázquez, 2023] evaluate the beam management framework of New Radio for LEO NTNs, finding that satellite tracking can be performed easily and that initial beam sweeping may only take a few seconds. However, their simulations assume a rather optimistic satellite pass (i.e., it always passes over the zenith of the CT) and rather high minimum elevation angles (68 and 51 degrees).

SpaceX's Starlink system also requires that its CTs must perform a beam sweeping procedure to enter the network. According to [Kutkov, 2023], the Starlink CT may enter the network in two modes: GNSS-assisted or via Starlink positioning. The author states that network entry is relatively fast when GNSS is available, but can be significantly slower when relying solely on Starlink positioning. Additionally, the report indicates that Starlink positioning is not yet functional for CTs on moving platforms.

The present paper makes the following contributions:

- It introduces HOOC-EM, an efficient beam-sweeping strategy for LEO mega-constellation CTs, which pixelates the celestial sphere using hexagonal and pentagonal sectors based on beamwidth. HOOC-EM incorporates satellite dynamics to develop an empirical Markov transition matrix based on constellation simulations. This matrix is used to determine the initial probability density function (PDF) of the sectors. Then the Markov transition matrix is used to update the sector probabilities during beam sweeping to account for satellite dynamics during the search.
- It provides numerical simulations to demonstrate the effectiveness of HOOC-EM, showing that the time for beam sweeping can range from less than a second to several tens of seconds, depending on the beamwidth and simulated scenario. HOOC-EM is shown to perform better than a traditional raster scan as well as two other methods that use the same hexagonal and pentagonal sectors when the Markov model is recent.

The remainder of this paper is organized as follows. Section II contains assumptions about the broadband LEO system that will be used throughout the paper. Section III describes the HOOC-EM algorithm in detail. Section IV provides a description of the simulations conducted and shows associated results. Section V gives conclusions about the study.

Notation

Column vectors are denoted with lowercase bold, e.g., $\boldsymbol{x}$. Scalars are denoted without bold, e.g., x. The nth entry of a vector $\boldsymbol{x}$ is denoted $x(n)$. Matrices and tensors are also denoted with bold, e.g., $\boldsymbol{X}$. For a tensor, the mth ith kth entry is $X_{mi}(k)$, the mth ith vector is $\boldsymbol{X}_{mi}$, and the mth matrix is $\boldsymbol{X}_m$. Zero-based indexing is used throughout the paper.

II. BROADBAND LEO SYSTEM DESCRIPTION

In this paper, a conceptual LEO broadband constellation will be assumed. The constellation may be a dedicated communications network such as SpaceX's Starlink system, or a fused LEO GNSS system as described by [Iannucci and Humphreys, 2022]. In either case, the CT must be granted access to the network at initial network entry (INE). To enter the network, the CT must have some *a priori* knowledge about the network as a whole. This section discusses the necessary assumptions this paper makes about the LEO network to enable HOOC-EM and, ultimately, full network entry.

1. Constellation Design Assumptions

In general, the CT does not need to make any assumptions about the design of the constellation. HOOC-EM is agnostic to the type of constellation, inclination angle, and even altitude. If necessary, this method could be performed on MEO and GEO constellations as well. However, since LEO is the forerunner in space-based broadband communications, this paper will focus on a LEO constellation.

Although a specific type of constellation is not required, some *a priori* information about the constellation could speed up network entry. For example, a given constellation over a given period of time may have certain azimuths and elevations that are more frequently occupied by satellites at certain latitudes. This sort of knowledge about the constellation could be used to construct a PDF that would enable a maximum-likelihood, satellite search that could take the place of a brute-force, blind satellite search. This concept is the foundation of HOOC-EM and will be the focus of this paper, with detailed discussion provided in Section 3.

2. Network Architecture Assumptions

This paper makes the following assumptions about the network. First, it is assumed that the transmitting satellites send downlink signals via directional beams, as is done by Starlink, OneWeb, and Iridium [Humphreys et al., 2023], [Blázquez-García et al., 2023], [Maine et al., 1995]. Consequently, some of the terminology described in [Qin et al., 2023] will be used in this paper as well. In particular, the terms "service cell," "assigned beam," and "fixed assigment interval" are of importance and will be redefined here. A service cell refers to the coverage area of a satellite beam, with the center of the service cell determined by user demand. An assigned beam is a beam directed by a satellite toward a designated service cell. A fixed assignment interval (FAI) is the interval of time over which beam assignments remain fixed across the constellation. The broadband network will be assumed to have an FAI of T_{FAI} seconds, during which a satellite transmitting an assigned beam will service the same service cell. Note that multiple satellites may be transmitting assigned beams to a given service cell. The transmitted signals within these beams are assumed to be orthogonal in at least two dimensions out of a possible four: frequency, time, polarization, and direction (azimuth and elevation). For example, each assigned beam is assumed to always be orthogonal in direction, but may share one or more of the other dimensions–frequency, time, or polarization.

The satellites may operate in either a bent-pipe (transparent) or regenerative configuration. The data and synchronization sequences sent in an assigned beam are assumed to be diverse in both frequency and time. A specific combination of frequency and time will denote a channel, and the data sent on that channel can be modulated in any way the network chooses. For example, Starlink uses orthogonal frequency division multiplexing (OFDM) and Iridium uses differentially encoded quadrature phase shift keying (DEQPSK) [Humphreys et al., 2023], [Maine et al., 1995]. Regardless of the modulation scheme, it is assumed that the transmitted signal contains a pilot or synchronization sequence of some kind. While these sequences reduce overall data capacity, they are necessary for channel equalization and symbol timing recovery. Additionally, they can be used in a matched filter for signal detection.

Finally, it is assumed that the network dedicates a time-slot specifically for network entry. In this slot the satellite transmits what is known as the synchronization signal. This signal is known to the CT and can be used within a matched filter to aid in signal detection during the beam sweeping procedure. The synchronization signal will be transmitted only every T_{SS} seconds. Note that the duration of the synchronization signal will be much shorter than T_{SS}. The remainder of the frame is assumed to be occupied by data. The synchronization periodicity T_{SS} should be large compared to the time offset caused by the distance between the satellite and the CT to enable the CT ample time for detection.

Furthermore, this paper will assume that the CT is in an area with a high number of users. That is, the CT will be in a service cell that is always illuminated by at least one transmitting satellite at some frequency band and polarization.

3. Customer Terminal Assumptions

Whenever the CT is powered on, INE will happen on a dedicated frequency band and polarization pair known to the CT. There will only be one satellite transmitting on that frequency band and polarization, specifically for INE. However, the location of that satellite is unknown to the CT when it is powered on, necessitating a satellite search in azimuth and elevation.

The CT is assumed to be equipped with a phased antenna array capable of steering a narrow beam to a desired azimuth and elevation. The array is assumed to be capable of beam width modulation, i.e., it can electronically generate beams of arbitrary beamwidths (using the definition of 3 dB beamwidth shown in Fig. 1). The CT is assumed to possess the necessary RF chains and associated hardware (low-noise amplifier, down-converter, analog to digital converter, etc.) to effectively use a phased array antenna. Additionally, the CT will have an inertial measurement unit (IMU) and a magnetometer to determine its orientation relative to the local East-North-Up coordinate frame. While the CT will be assumed to also have an onboard GNSS receiver, the receiver will be assumed inactive or inoperable in this paper. Many existing systems, including SpaceX's Starlink rely on GNSS for fast network entry. This critical reliance would have severe consequences if GNSS were unavailable, onboard receivers fail, or if there is a system-wide GNSS fault. Therefore, it is important to begin developing GNSS-free technology moving forward.

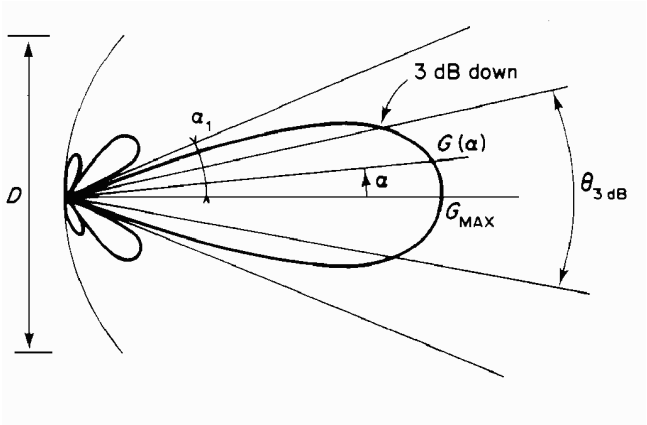

Figure 1: A notional polar plot of receiving antenna performance is provided to illustrate the definition of 3 dB beamwidth. The typical definition of beamwidth is defined at the 3 dB, or half power point [Maral et al., 2020]. In this context, D is the antenna diameter, α is an arbitrary angle defined from the max power point G_{max}, and $G(\alpha)$ is the gain at α.

III. HOOC-EM ALGORITHM

The HOOC-EM algorithm is a multistage process that begins with defining an appropriate search space. Then, using knowledge of the network of interest, probabilities are assigned to the defined search space. The search space and associated probabilities are then applied to the beam sweeping problem. This section deals with each of these steps in detail.

1. Search Space

The HOOC-EM algorithm begins with defining a suitable search space. For space-to-Earth communications, it is often convenient to consider the space above the observer as a sphere with the observer at its origin. This approach leverages the fact that objects in space move in curvilinear motion. This sphere, referred to as the observer's celestial sphere, will be the search space of interest moving forward.

Most current beam sweeping approaches consider a raster scan of azimuths and elevations. A raster scan consists of searching each azimuth for a given elevation and so on. A traditional raster scan of azimuth and elevation does not account for the spherical nature of the search space (e.g., at an elevation of 90 degrees it is unnecessary to search the full 360 degrees of azimuth), resulting in a prohibitively large search. A method that uses fewer search points while still maintaining full coverage should be considered instead.

To ensure full coverage with a minimal number of points, it is useful to consider various methods of partitioning a sphere. Historically, partitioning the celestial sphere has been valuable for remote sensing applications, as it facilitates convenient computer processing [Chan, 1980, Tegmark, 1996, McCollum, 2001]. In these approaches, having numerous points within partitions of equal area was desirable. For the present use case, having fewer points is advantageous, but equal partitions are especially desirable as they better represent constant beamwidths.

Given that a large number of points is not required for this application, the centroid of each partition can be selected, with the

partition area approximated to match the desired beamwidth. This approach will be employed in this paper.

Next, an appropriate partitioning scheme must be selected. The partitioning methods developed in the aforementioned papers all adequately segment the celestial sphere. To select among them, it is important to consider how the CT's beam intersects with the celestial sphere. The cross section is predominantly circular, with some flattening as elevation approaches 0 degrees. Therefore, a partitioning scheme that approximates a circle should be favored. Scalability is also crucial: the partitioning scheme should be capable of being scaled down to represent an arbitrarily small beamwidth.

With these criteria in mind, Table 1 provides a brief overview of each partioning scheme. It is clear from the table that the hexagonal partioning scheme demonstrated by [McCollum, 2001] is the most suitable for the present use case. In contrast, the square partitioning scheme developed by [Chan, 1980] is the least favorable, as it lacks scalability. While some more recent work has developed scalable square partitioning schemes [Dimitrijević et al., 2016], they stil fall short of the hexagonal scheme for the present use case in terms of area efficiency. The triangular scheme, or icosahedral tiling, presented by [Tegmark, 1996] is also ill-suited for the present use case due to its area characteristics. As a result, this paper will use a hexagonal partitioning scheme.

Table 1: Partition Methods: Shape, Scalability, Coverage

Method	Shape	Scalability	Fraction of Circle
[Chan, 1980]	Square	No	$\frac{2}{\pi}$
[Tegmark, 1996]	Triangle	Yes	$\frac{3\sqrt{3}}{4\pi}$
[McCollum, 2001]	Hexagon*	Yes	$\frac{3\sqrt{3}}{2\pi}$

* Hexagons and exactly 12 pentagons.

It is important to note that the triangular and hexagonal scheme are intrinsically linked. All hexagonal partitions of a sphere begin as an ordinary unit icosahedron (a polyhedron with 20 triangular faces that is circumscribed within the unit sphere). To achieve a hexagonal partitioning, each edge of the ordinary icosahedron must be truncated at its midpoint. This process results in a truncated icosahedron, which consists of 20 hexagonal faces and 12 pentagonal faces. The resulting faces can then be projected onto the unit sphere to form the partitions. Since this paper is only concerned with the centroids of the partitions, it is sufficient to project the centroid of each face to the unit sphere. This will create partitions with approximately equal area. To map the area of these partitions to beamwidth, the approximate surface area in steradians of each partition may be calculated by

$$S_{\text{partition}} \approx \frac{4\pi}{N_{\text{faces}}} \tag{1}$$

where N_{faces} is the number of faces of the polyhedron. Then, the beamwidth in degrees is approximated as

$$\theta_{3\text{ dB}} \approx \sqrt{S_{\text{partition}}} \times \frac{180}{\pi} \tag{2}$$

For example, the truncated icosahedron would have partitions representing a beamwidth of $\theta_{3\text{ dB}} \approx 35.90$ degrees. This beamwidth is quite large. To further reduce it, we begin with the truncated icosahedron. The truncated icosahedron can be transformed back to a polyhedron with triangular faces by taking its dual. The dual operation consists of identifying the centroid of each face of a polyhedron and adding edges connecting each existing vertex to the centroid. The centroid is then projected to have unit distance from the origin, becoming a new vertex. Once the polyhedron has triangular faces again, it may be truncated as usual to produce a polyhedron with hexagonal and pentagonal faces once more. This may be repeated until the desired beamwidth is achieved. Algorithm 1 summarizes this process as an object-oriented program. The user inputs a number of iterations N_{iter} based on a desired beamwidth and the algorithm outputs a polyhedron object. The polyhedron object is initialized as a unit icosahedron and is truncated once before the loop begins. The polyhedron object has vertices, faces, and centers as members. It also has member functions `truncate()` and `dual()` that perform the respective operations on the vertices, faces, and centers of the object. The polyhedron object is dualed and truncated in a loop until the number of iterations equals the input.

Table 2 provides an overview of the characteristics of polyhedra resulting from various values of N_{iter}. The method allows for a wide range of beamwidth approximations, with finer resolution achievable at smaller beamwidths. Notably, the number of faces to search is significantly reduced compared to the points in a traditional raster scan. Interestingly, there are always 12 pentagonal faces, a consequence of Euler's characteristic, which precludes a sphere from being entirely tiled with hexagons [Euler, 1758]. Figure 2 shows an example of a polyhedron with triangular faces before and after truncation with $N_{\text{iter}} = 5$, showing both hexagonal and pentagonal faces.

Algorithm 1: `generatePolyhedron`

Input: N_{iter}

Output: `polyhedron`

```
polyhedron ← icosahedron
polyhedron.truncate()
for i = 2:N_iter do
    polyhedron.dual()
    polyhedron.truncate()
end
```

Table 2: Polyhedron Partitioning: Face and Beamwidth Analysis

N_{iter}	Faces	Hexagons	Pentagons	Beamwidth (degrees)	Raster Points
1	32	20	12	35.90	66
2	122	110	12	18.39	200
3	272	260	12	12.32	450
4	482	470	12	9.25	780
5	752	740	12	7.41	1225
6	1082	1070	12	6.17	1770
7	1472	1460	12	5.29	2415
9	2432	2420	12	4.11	3872
12	4322	4310	12	3.09	6903
14	5882	5870	12	2.64	9453

2. Assigning Probabilities

Once a suitable search space is defined, it is necessary to apply probabilities to each partition in order to perform a maximum likelihood search. The first step involves setting the probability of impossible search cells to zero. These cells can typically be identified by elevation: hexagonal and pentagonal sectors that fall below a minimum elevation angle should have their probabilities set to zero. The user may set this mask angle based on preference, though most networks will have a prescribed minimum elevation angle below which satellites will not transmit. For example, SpaceX's Starlink has a minimum elevation angle of 25 degrees for Ku-band operations, while Amazon Kuiper will require a minimum elevation angle of 35 degrees for their customer terminals [Space Exploration Holdings, 2020, Systems, 2019]. Adopting a network-based minimum elevation angle, when available, is advisable, as it can eliminate a significant portion of the search space. While a user-selected minimum elevation angle may also be effective, it risks creating a search space that is either too large or too small.

After reducing the total search space, an appropriate PDF is applied to the remaining search cells. One possibility would be to apply a uniform distribution to the search space, resulting in a completely random search. This would be a suboptimal strategy, as the probabilities would be poorly assigned. A significant improvement could be made by considering a common aspect of satellite communications: satellite networks prioritize transmitting from higher-elevation satellites as these signals have the highest received power. With this in mind, a more effective strategy might be to search higher elevation cells first, as they are more likely to contain a satellite. Since the CT might lack precise knowledge of the exact distribution relative to elevation, an assumed distribution (e.g., linear, exponential) would be necessary. Fig. 3 shows the truncated polyhedron from Fig. 2 with a minimum elevation angle of 35 degrees and a heat map applied according to uniform and linear elevation-based PDFs. The PDFs are mapped to a maximum-likelihood criterion, where 1 indicates the most likely cell and 0 the least likely cell. Clearly, the elevation-based PDF better approximates how communications satellites may transmit in practice. Thus, if the CT had no knowledge of its own network the best approach may be to apply a user-selected minimum elevation angle and use an elevation-based PDF. However, there are better strategies if recent knowledge of some network parameters is available.

When recent information about the state of the constellation is known to the CT, such as if the CT were recently powered off after connection to the network, a more advanced way of determining the PDF can be employed. This approach is crucial for ensuring the speed of the HOOC-EM algorithm. The technique goes as follows. Suppose the network consists of a constellation of satellites, each of which can be described by its position and velocity vectors $\boldsymbol{r}$ and $\boldsymbol{v}$, which may be propagated using a numerical integration technique. Consider also that the CT is placed at the origin of the spherical search space described previously and that each hexagonal partition is a cell to be searched in the initial beam sweeping procedure. By propagating the positions and velocities of the satellites within the constellation over a chosen duration, one can record the cell location of each satellite at each time epoch. Using a frequentist approach, the probability density of each cell of the search space can then be inferred. Let N be the total number of hexagonal and pentagonal cells in the search space, $p(i)$ be the probability that the ith

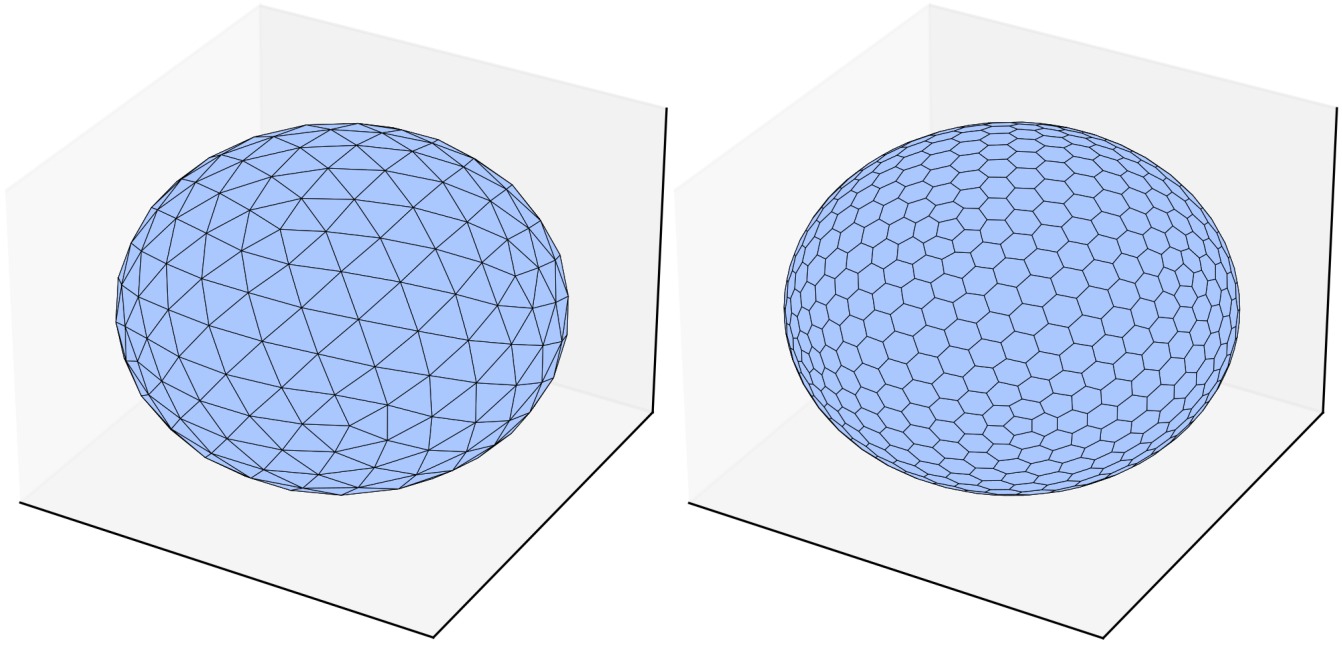

Figure 2: A polyhedron with triangular faces after $N_{\text{iter}} = 5$ iterations (left) and the same polyhedron after the `truncate()` operation is performed (right), showing both hexagonal and pentagonal faces.

cell is occupied by at least one satellite, and $n(i)$ be the number of epochs in which the ith cell has been occupied by at least one satellite. The approximation of $p(i)$ is then given by

$$p(i) \approx \frac{n(i)}{\sum_{j=0}^{N-1} n(j)}, \quad i \in \{0, 1, \ldots, N-1\} \tag{3}$$

The complete set of N probabilities forms the PDF of the search space and will be denoted by $\boldsymbol{p} = [p(0), p(2), \ldots, p(N-1)]^{\mathsf{T}}$. Since the satellites in view and their respective azimuths and elevations vary with the CT's latitude, this estimation must be repeated for each latitude where satellites are visible, given that the location of the CT is unknown when it is initially powered on. The resulting PDF for a given latitude λ will be denoted by $\boldsymbol{p}_\lambda = [p_\lambda(0), p_\lambda(1), \ldots, p_\lambda(N-1)]^{\mathsf{T}}$.

If the position of the CT remains unknown after powering on, latitude should be marginalized out of the PDF. This can be done by assigning a PDF to the possible latitudes of the CT, potentially using population density data. Since the CT lacks knowledge of its location, it can most reasonably estimate its latitude by where it is most likely to be powered on: where there are more people. The PDF may be determined by dividing the population density at each latitude by the total population accounted for in the data. For example, Fig. 4 shows the resulting PDF L_λ when this procedure is applied to population density data from [Kummu and Varis, 2011]. Finally, latitude can be marginalized out by

$$p(i) = \sum_{\lambda=\lambda_{\text{min}}}^{\lambda_{\text{max}}} \sum_{i=0}^{N-1} L_\lambda p_\lambda(i) \tag{4}$$

Now that a PDF has been obtained, assigning probabilities to each cell in the search space according to likely satellite positions and independent of latitude, it is still not appropriate to use this PDF directly in a maximum likelihood search. While this PDF will adequately describe where satellites are likely to be located, it does not account for where they are likely to be transmitting. To address this, consider that satellites are more likely to transmit at higher elevations. Therefore, a more suitable PDF would be a joint PDF that considers both satellite position and elevation. To determine the joint pdf, the previously obtained PDF $\boldsymbol{p}$ and an elevation-based PDF like what is shown in Fig. 3, which will be denoted by $\boldsymbol{e} = [e(0), e(1), \ldots, e(N-1)]^{\mathsf{T}}$ are combined. Note that $\boldsymbol{e}$ will have its highest probability at the cell at the zenith angle relative to the CT and the probability will decrease as relative elevation angles of the cells decrease until the elevation angles of the cells drop below some minimum elevation angle el_{min}. All cells below that elevation angle will have a probability of 0. Since $\boldsymbol{e}$ is already conditioned on the hexagonal cells of the search space, the ith element of the joint PDF $\boldsymbol{x}$ can be calculated by an element-wise multiplication and normalization as

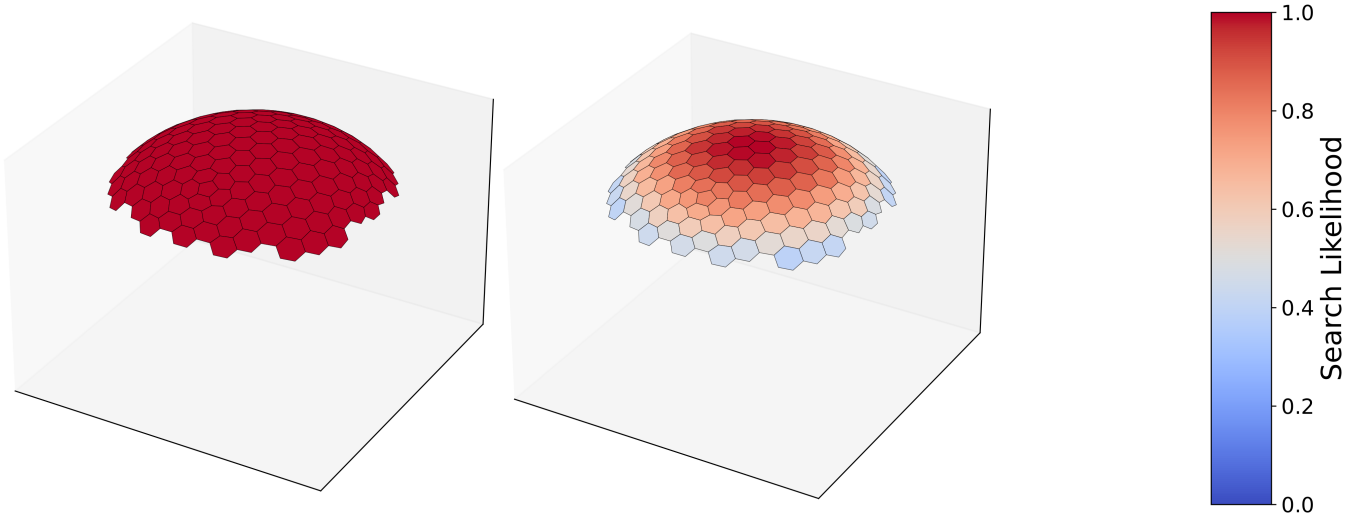

Figure 3: A heat map of the truncated polyhedron from Fig. 2 after applying a minimum elevation angle of 35 degrees and a uniform (left) and elevation-based (right) probability density function. The probability density function is mapped to a maximum-likelihood search criterion, applying a search likelihood of 1 to the most probable cells and 0 to the least probable.

$$x(i) = \frac{p(i)e(i)}{\sum_{i=0}^{N-1} p(i)e(i)} \tag{5}$$

Further improvement of this joint PDF could be made if even more specific network information was known to the CT, but that is outside the scope of this paper as this information could vary significantly between networks.

The current iteration of the PDF $\boldsymbol{x}$ is now a very good representation of the true PDF of the search space. However, it still fails to account for satellite dynamics. Indeed, a maximum-likelihood search for the best beam pair will likely span multiple time epochs, yet the current PDF only captures a single moment in time. While (3) marginalizes over time to address the CT's lack of knowledge regarding the true time at power-on, this approach is insufficient for an extended search process.

Over the course of a maximum likelihood search, searched cells are set to 0 probability to prevent them from being searched again. Due to the nature of satellite dynamics, permanently assigning 0 probability to a searched cell for the remainder of the search can be erroneous. Over time, the probability that a previously searched cell will be reoccupied by a transmitting satellite increases as satellites transition from one cell to another.

To better model this dynamic behavior, a Markov model is employed. Since the exact time is unknown and higher-order terms in the satellite dynamics model are not accounted for, the transitions of satellites between cells may be considered stochastic from the perspective of the CT. This approach allows for a more accurate representation of the evolving probabilities throughout the search process, leading to improved search efficiency and accuracy. Fortunately, the transition probabilities can be determined during the same simulations used to compute $\boldsymbol{p}_\lambda$, noting that transition probabilities will depend on latitude as well. Let $\boldsymbol{M}_\lambda$ be the Markov transition matrix at latitude λ and $M_{\lambda,i}(j)$ be the probability that a satellite transitions from the ith cell to the jth cell at latitude λ. The stochastic matrix $\boldsymbol{M}_\lambda$ would be assembled as

$$\boldsymbol{M}_\lambda = \begin{bmatrix} M_{\lambda,0}(0) & M_{\lambda,0}(1) & \dots & M_{\lambda,0}(N-1) \\ M_{\lambda,1}(0) & M_{\lambda,1}(1) & \dots & M_{\lambda,1}(N-1) \\ \vdots & \vdots & \ddots & \vdots \\ M_{\lambda,N-1}(0) & M_{\lambda,N-1}(1) & \dots & M_{\lambda,N-1}(N-1) \end{bmatrix} \tag{6}$$

The elements of $\boldsymbol{M}_\lambda$ can be approximated through numerical simulations of the constellation in a similar way to $\boldsymbol{p}_\lambda$ in (3). Specifically, the matrix $\boldsymbol{A}_\lambda$ can be assembled with elements $A_{\lambda,i}(j)$, which are the number of times any satellite has transitioned from the ith cell to the jth cell at latitude λ. The matrix $\boldsymbol{A}_\lambda$ is assembled in the same way as in (6). Although $\boldsymbol{A}_\lambda$ is not needed for any mathematical operations in matrix form, its matrix representation is convenient for data storage. Then, each element of

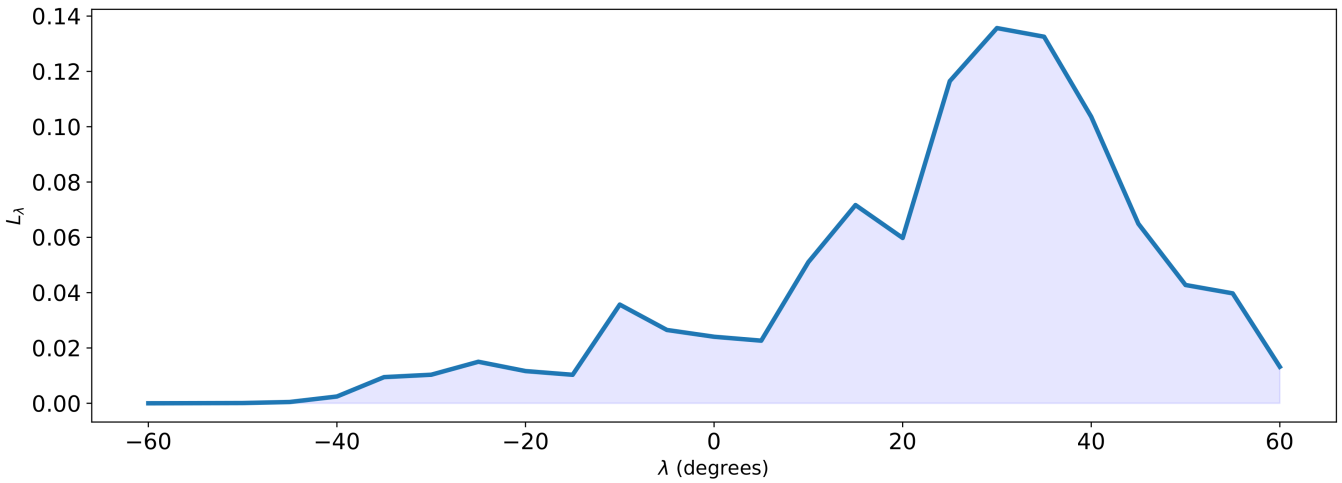

Figure 4: PDF of the CT latitudes determined by data from [Kummu and Varis, 2011].

$\boldsymbol{M}_\lambda$ can be approximated as

$$M_{\lambda,i}(j) \approx \frac{A_{\lambda,i}(j)}{\sum_{k=0}^{N-1} A_{\lambda,i}(k)}, \quad i,j \in \{0,1,\ldots,N-1\} \tag{7}$$

Additionally, the corresponding matrix $\boldsymbol{M}_\lambda$ can be marginalized for latitude by approximating $M_{i,j}$ using $\boldsymbol{A}$, the marginalized version of $\boldsymbol{A}_\lambda$. The procedure is the same as in (4)

$$\boldsymbol{A} = \sum_{\lambda=\lambda_{\text{min}}}^{\lambda_{\text{max}}} L_\lambda \boldsymbol{A}_\lambda \tag{8}$$

The transition probabilities $M_i(j)$ can then be approximated as in (7). Interestingly, the extraction of the Markov transition matrix eliminates the need to calculate $\boldsymbol{p}$ directly. Instead, $\boldsymbol{p}$ can be derived from $\boldsymbol{M}$. Recognizing that $\boldsymbol{M}$ is a positive stochastic matrix, it follows that 1 is an eigenvalue of $\boldsymbol{M}$, with all other eigenvalues having absolute values less than 1. By the Perron-Frobenius theorem, $\boldsymbol{M}$ must admit a unique normalized steady state vector, which spans the 1-eigenspace [Robinson, 2002]. That is, the steady state solution of the difference equation

$$\boldsymbol{\pi}^\mathsf{T} = \boldsymbol{\pi}^\mathsf{T} \boldsymbol{M} \tag{9}$$

exists and serves as a valid PDF. This solution represents the steady state behavior of the Markov model, corresponding to the probabilities that the cells in the search space contain at least one satellite, which is the definition of $\boldsymbol{p}$.

Algorithm 2 summarizes the process of assigning probabilities to the search space in HOOC-EM, structured as an object oriented program. The program takes as input the polyhedron object generated from Algorithm 1, and a constellation object with `simulate()` and `count()` member functions. The `simulate()` function simulates the constellation for a duration T seconds with an update period of Δt seconds, recording the states of each satellite in the constellation at each time epoch. The `count()` function tracks the number of transitions between the cells of the polyhedron object according to a specified latitude λ.

Additional inputs include the simulation duration T, the update period Δt, and minimum and maximum latitudes λ_{min} and λ_{max}, respectively. The algorithm outputs $\boldsymbol{p}$ and $\boldsymbol{M}$ for use in the subsequent search algorithm.

3. HOOC-EM Search

Once the search space has been defined and probabilities have been assigned, the search can begin. The search proceeds as a typical maximum likelihood search, where the algorithm will search the cell with the highest probability in the PDF and so on. The slight difference is in the inclusion of the Markov model, which will continually update the PDF as the search continues.

It is important to note that the Markov transition matrix must be relatively recent to enable HOOC-EM. In the event of a complete cold start, the CT would first perform an elevation-based search to initiate network entry. Afterwards, and for as long as the CT

Algorithm 2: `assignProbabilities`

Input: `polyhedron`, `constellation`, T, Δt, λ_{min}, λ_{max}
Output: $\boldsymbol{p}$, $\boldsymbol{M}$

`constellation.simulate(`T, Δt`)`
$\boldsymbol{A} \leftarrow$ `zeros(`N, N`)`
for $\lambda = \lambda_{\text{min}} : \lambda_{\text{max}}$ **do**
    $\boldsymbol{A}_\lambda =$ `constellation.count(polyhedron,`λ`)`
    $\boldsymbol{A} \mathrel{+}= L_\lambda \boldsymbol{A}_\lambda$ `/* From (8)` `*/`
end
$\boldsymbol{M}$ = `calcMarkovMatrix(`$\boldsymbol{A}$`) /* From (7)` `*/`
$\boldsymbol{p}$ = `calcPDF(`$\boldsymbol{M}$`) /* Solution to (9)` `*/`

is connected to the network, the network will furnish 'fresh' Markov transition matrices with which the CT can use to perform HOOC-EM if it is powered off and then powered on in quick succession. How 'fresh' the Markov transition matrix needs to be still needs to be studied but the results presented in Section IV indicate that the Markov matrix is still effective after at least one orbital period.

Algorithm 3 provides a programatic explanation of the maximum likelihood search used in HOOC-EM. The algorithm accepts the following inputs: a `searchSpace` object, which can represent an entire polyhedron or a reduced version after applying a minimum elevation angle; $\boldsymbol{x}$, the PDF; and $\boldsymbol{M}$, the Markov transition matrix. Note that $\boldsymbol{x}$ and $\boldsymbol{M}$ both apply to the entire polyhedron, as opposed to just the search space. This is because the transitions that would occur at the edges of the search space would be more difficult to model. Besides, $\boldsymbol{x}$ will only have probabilities greater than 0 above the minimum elevation angle anyway due to the application of the elevation-based PDF earlier.

The algorithm begins by identifying the index of the cell with the highest probability. The probability of that cell is then set to zero. The `searchCell()` function determines the azimuth and elevation of the center of that cell, points the beam of the antenna array at that azimuth and elevation, reads samples from the ADC, and correlates them with a local replica of the synchronization signal and measures the resulting signal power. If the power exceeds a certain threshold, detection is returned as **True**, ending the loop, and azimuth and elevation are returned as 'az' and 'el', respectively. If the power is below the threshold, detection is returned as **False** and the PDF is updated using the Markov transition matrix. The process then continues until detection is **True**. The azimuth and elevation are returned for satellite tracking purposes later on.

Algorithm 3: `maximumLikelihoodSearch`

Input: `searchSpace`, $\boldsymbol{x}$, $\boldsymbol{M}$
Output: az, el

detection $\leftarrow$ **False**
while !detection **do**
    $i =$ `arg max(`$\boldsymbol{x}$`)`
    $\boldsymbol{x}(i) = 0$
    detection, az, el = `searchCell(searchSpace,`i`)`
    $\boldsymbol{x} = \boldsymbol{x}\boldsymbol{M}$
end

Finally, the HOOC-EM algorithm can be developed. Algorithm 4 outlines the program as an object oriented program with Algorithms 1, 2, and 3 featured as functions. Of note there are the functions `calcJointPDF()` and `applyMinimumElevationAngle()`. The function `calcJointPDF()` performs the operation shown in (5) by first generating the PDF $\boldsymbol{e}$, taking into account the minimum elevation angle el_{min}. The function `applyMinimumElevationAngle()` removes all cells with centers below the elevation angle el_{min} from the search space.

IV. SIMULATIONS AND RESULTS

HOOC-EM can now be tested using an exemplar communications constellation. This paper will use an approximation of the Amazon Kuiper-Ka constellation for testing. The exact parameters used in the constellation are taken from [Systems, 2019]. The constellation is a LEO constellation with 3 orbital shells at different altitudes and inclination angles. Table 3 shows the given parameters for each orbital shell. The exact parameters for simulation of the constellation are not given, but it is claimed that the constellation will have good coverage between 56 degrees north and south of the Equator. One way to achieve this would be to simulate each shell as a Walker Delta constellation. That is the approach taken in this paper.

Algorithm 4: HOOC-EM

Input: N_{iter}, `constellation`, T, Δt, λ_{min}, λ_{max}, el_{min}

Output: az, el

`polyhedron` = `generatePolyhedron(`N_{iter}`)` `/* Algorithm 1 */`

$\boldsymbol{p}, \boldsymbol{M}$ = `assignProbabilities(polyhedron, constellation,` $T, \Delta t, \lambda_{\text{min}}, \lambda_{\text{min}}$`)` `/* Algorithm 2 */`

$\boldsymbol{x}$ = `calcJointPDF(`$\boldsymbol{p}, \text{el}_{\text{min}}$`)` `/* From (5) */`

`searchSpace` = `applyMinimumElevationAngle(polyhedron,` el_{min}`)`

az, el = `maximumLikelihoodSearch(searchSpace,` $\boldsymbol{x}, \boldsymbol{M}$`)` `/* Algorithm 3 */`

Table 3: Simulated Constellation: Altitudes and Inclinations [Systems, 2019]

Altitude (km)	Inclination (deg)	Planes	Number of Satellites per Plane	Number of Satellites
590	33	28	28	784
610	42	36	36	1296
630	51.9	34	34	1156

Using the Walker Delta constellation, the COE of each satellite can be determined. Using the COE each satellite can be propagated forward in time using a numerical integration technique. For the purposes of assigning probabilities, the constellation will be propagated using the two-body model with no perturbations. The two-body model has an analytical solution and is periodic with one orbital period. After rotating to the Earth-centered, Earth-fixed (ECEF) coordinate system, the constellation will be exactly periodic after a number of sidereal days that are evenly divisible by the orbital period. Furthermore, emerging communications constellations often consist of multiple shells, like the Kuiper-Ka constellation. As a result, the constellation will only be exactly periodic after a number of sidereal days that are evenly divisible by the greatest common multiple of the three orbital periods. This, of course, would be prohibitively long to simulate. Therefore, this paper will only consider one orbital period for testing. That is, the resulting PDF and Markov transition will only be good to one orbital period of the constellation or approximately 80 minutes in the case of the Kuiper-Ka constellation. Let $\boldsymbol{r} = [x, y, z]^{\text{T}}$ be the position state vector of a satellite in the Earth-centered, inertial (ECI) frame, μ be the standard gravitational parameter for Earth, $||.||_2$ be the standard Euclidean norm, and $f(t, \boldsymbol{r}, \dot{\boldsymbol{r}})$ be unmodeled, time-dependent perturbations. Then the two-body equations of motion are

$$\ddot{\boldsymbol{r}} = -\frac{\mu}{||\boldsymbol{r}||_2^3}\boldsymbol{r} + f(t, \boldsymbol{r}, \dot{\boldsymbol{r}}) \tag{10}$$

Now (10) may be propagated using a numerical integration technique. Fig. 5 shows the constellation described in Table 3 propagated over one orbital period. In addition, the average number of satellites above a 35 degree minimum elevation angle is shown as a function of latitude, showing strong correspondence to the same chart shown in [Systems, 2019].

Using the simulated constellation in Fig. 5, the positions of the satellites are rotated from the ECI frame to the ECEF frame and the probabilities are assigned as in Subsection III.2 to the polyhedra described in Table 2 with a minimum elevation angle of 35 degrees and the joint PDF is determined using an exponential, elevation-based PDF. Let beamwidth in degrees be β, then Fig. 6 shows the resulting probability density functions mapped to each search space delineated by their beamwidth according to a maximum likelihood criterion assigning the highest probability cell a 1 and decreasing as probability of each cell decreases.

1. Simulations

Once the probabilities are assigned, Monte Carlo simulations are carried out to verify the efficacy of HOOC-EM. The Monte Carlo simulations are performed as follows. The constellation is simulated using the two-body model over one orbital period. However, for the purposes of the Monte Carlo simulation the J_2 perturbation will modeled and included in the simulation of the constellation. This is to serve as a stand-in for unmodeled perturbations when determining the Markov transition matrix $\boldsymbol{M}$ at the control segment. The most significant perturbing accelerations for a LEO satellite are due to Earth's non-uniform gravity. The most severe of which are the zonal terms denoted as J_2 [Curtis, 2009]. Let R_e be the mean radius of the Earth and $J_2 = 1.08262668355 \times 10^{-3}$ be the dimensionless zonal coefficient. The resulting equations of motion of each axis of a LEO satellite in the ECI frame are [Morales et al., 2019]

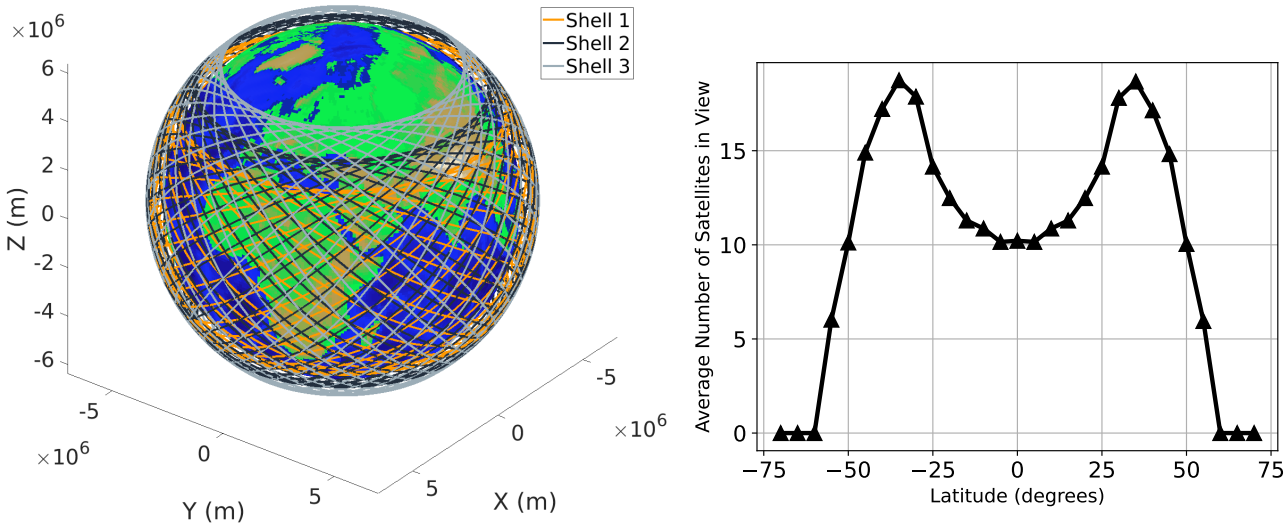

Figure 5: The simulated LEO constellation shown above Earth (left) and the average number of satellites in view (above a 35 degree elevation angle) at different latitudes (right) determined at increments of 5 degrees with each increment denoted by a triangle.

$$
\begin{aligned}
\ddot{x} &= \frac{-\mu x}{||\boldsymbol{r}||_2^3}\left[1 + J_2\frac{3}{2}\left(\frac{R_e}{||\boldsymbol{r}||_2}\right)^2\left(1 - 5\frac{z^2}{||\boldsymbol{r}||_2^2}\right)\right] \\
\ddot{y} &= \frac{-\mu y}{||\boldsymbol{r}||_2^3}\left[1 + J_2\frac{3}{2}\left(\frac{R_e}{||\boldsymbol{r}||_2}\right)^2\left(1 - 5\frac{z^2}{||\boldsymbol{r}||_2^2}\right)\right] \\
\ddot{z} &= \frac{-\mu z}{||\boldsymbol{r}||_2^3}\left[1 + J_2\frac{3}{2}\left(\frac{R_e}{||\boldsymbol{r}||_2}\right)^2\left(3 - 5\frac{z^2}{||\boldsymbol{r}||_2^2}\right)\right]
\end{aligned}
\tag{11}
$$

The equations in (11) are integrated using a numerical integration technique with the Walker Delta initial conditions for each satellite. The positions of each satellite in the constellation are then saved. At the beginning of each Monte Carlo simulation a random time within the orbital period is selected and the constellation is propagated from that time. The position of the CT is randomly selected; the latitude of the CT is randomly selected according to the PDF given in Fig. 4, the longitude is selected from a uniform distribution from -180 to 180 degrees, and the altitude is chosen to be 800 m, which is the average height of land above sea level. Among the visible satellites, one is selected to be transmitting at the beginning of the simulation according to the elevation-based PDF in Fig. 3. The selected satellite will remain transmitting for the fixed assignment interval T_{FAI} seconds. Afterwards a new satellite will be selected using the same criterion and will transmit for T_{FAI} seconds and so on. During this time searches will be going on with the following methods: (1) a raster scan of azimuths and elevations, beginning with zenith (2) a maximum likelihood search with the uniform PDF from Fig. 3, (3) a maximum likelihood search with the elevation-based PDF from Fig. 3, and (4) HOOC-EM using the PDFs from 6 that are propagated using the Markov models derived from earlier simulations of the constellation. Note that each method is performed at the beamwidths shown in Fig. 6 and the uniform and elevation-based PDFs are equivalently mapped to the corresponding polyhedra. This proceeds until a detection or acquisition is made.

The acquisition criterion is that the transmitting satellite is within the cell that the antenna of the CT is pointing at during the period T_{FAI}. While no explicit signal power criterion is used here it can be argued that the network may design their signal to function with a given beamwidth. For example, it was shown in [Komodromos et al., 2023] that an OFDM signal may be detected at SNRs as low as -43 dB when the synchronization sequence encompassed the entire Starlink frame. While this would be unreasonable in practice, as no data would be broadcast, it shows how detection at a certain antenna gain or beamwidth could be considered a signal design parameter. Furthermore, the present approach could be argued to be conservative. If a detector based on pure SNR were used a satellite may be detected in adjacent hexagonal cells, depending on the position of the satellite.

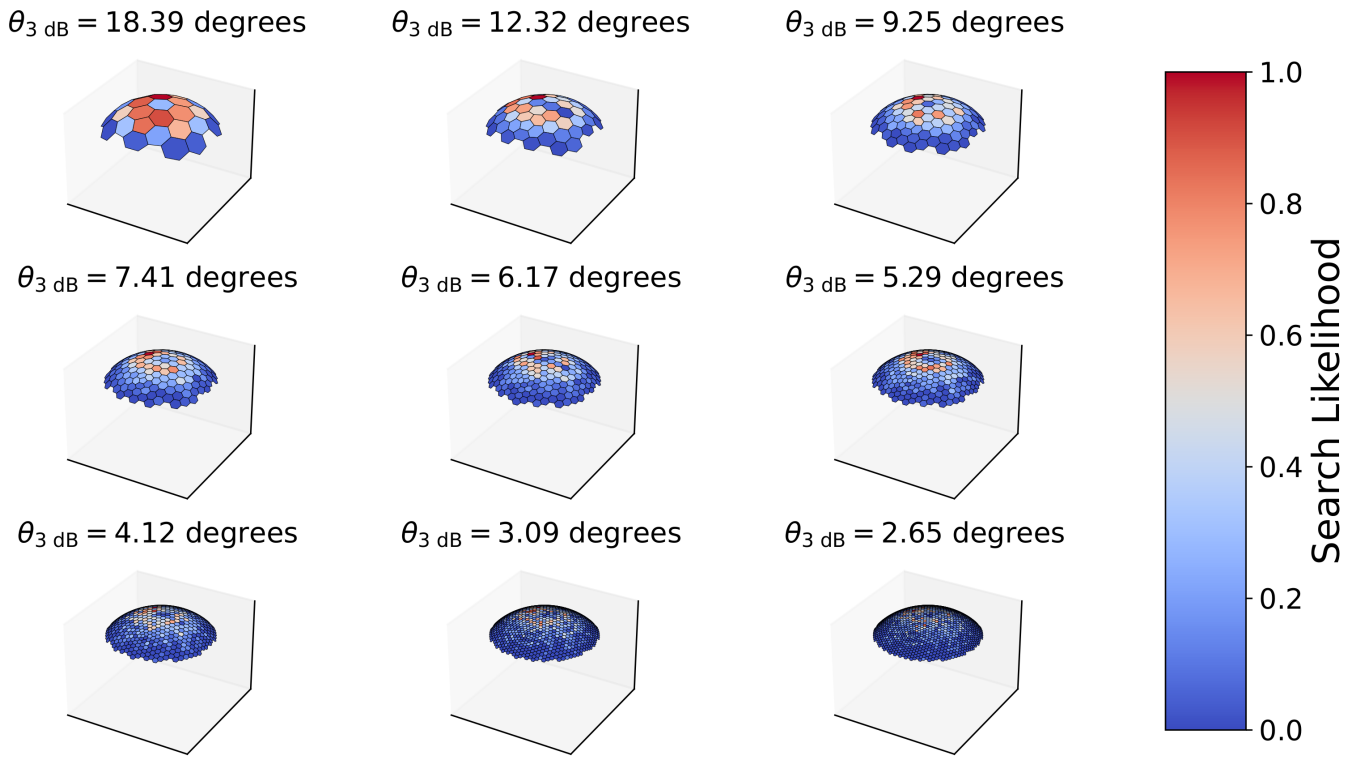

Figure 6: The empirical satellite-and-elevation-based probability density functions, marginalized for latitude, applied to the hexagonal and pentagonal sectors above a 35 degree elevation mask for beamwidths from 2.65 to 18.39 degrees.

2. Results

The simulations were performed with $T_{\mathrm{FAI}} = 5$ and 15 seconds. A T_{FAI} of 15 seconds aligns with observations of the Starlink network in [Qin et al., 2023], while a shorter T_{FAI} of 5 seconds could be employed by a future fused LEO GNSS as shorter assignment intervals would allow for greater geometric diversity and reduce the time to first fix. Fig. 7 shows the results of a 500 run Monte Carlo simulation at $T_{\mathrm{FAI}} = 5$ seconds.

On the left, the average time to detection in seconds is plotted against beamwidth in degrees. It clearly shows that the raster scan is the least effective approach, even underperforming compared to the uniform search with hexagonal tiling, which benefits from fewer search points. For wider beamwidths, the elevation-based and HOOC-EM approaches perform similarly, likely due to fewer search points and the reduced likelihood of satellite transitions in larger hexagonal cells. However, as beamwidths narrow–where satellite transitions are more frequent and the number of search points increases–HOOC-EM demonstrates superior performance, which is crucial in high-interference scenarios requiring narrow beams.

On the right, the cumulative density functions (CDFs) for a beamwidth of 2.64 degrees are displayed, further highlighting the inferiority of the uniform and raster scan approches. The elevation-based and HOOC-EM searches perform similarly for the first 50% of the searches, but beyond this, the elevation-based approach shows multiple plateaus. At this assignment interval and beamwidth, over 90% of the HOOC-EM searches finish in under 40 seconds, while the elevation-based search has much longer tails, with over 10% of the searches taking over a minute to perform. Fig. 8 shows the results when $T_{\mathrm{FAI}} = 15$ seconds. The results are very similar to those shown in Fig. 7, with a general reduction in average detection time. This improvement occurs because the search is more likely to finish before the transmitting satellite switches beams. Overall the trends remain consistent: the raster scan and uniform searches are the slowest, while the elevation-based and HOOC-EM searches are the fastest, with the HOOC-EM search edging out the elevation-based search at narrow beamwidths.

On the right, the CDFs for a beamwidth of 2.64 degrees are shown. The elevation-based and HOOC-EM searches perform similarly up to just over 60% of the searches. At this assignment interval and beamwidth, over 90% of the HOOC-EM searches take under 30 seconds to complete, compared to over 10% of the elevation-based searches taking over 50 seconds to complete. If the user has some information about the position of the CT, performance can be improved significantly improved. Fig. 9 shows the results at a known position for elevation-based and HOOC-EM searches at $T_{\mathrm{FAI}} = 15$ seconds. The Markov matrix $\boldsymbol{M}$ was determined by a simulation of the constellation over one orbital period with the CT at the known position. With knowledge of

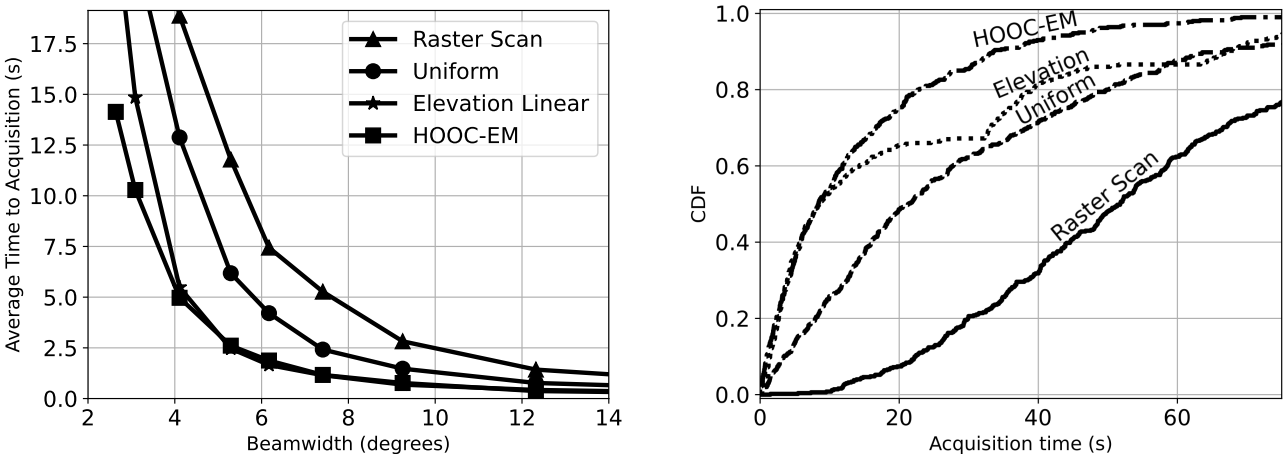

Figure 7: The average time to detection of the various beam sweeping methods (left) and their cumulative density functions (right) at a beamwidth of 2.64 degrees with $T_{\text{FAI}} = 5$ seconds.

the position of the CT, the HOOC-EM search is convincely better than the elevation-based search in terms of average time to detection. On the right, the CDFs for both searches at a beamwidth of 2.64 degrees are shown. Nearly 99% of the HOOC-EM searches complete in just under 20 seconds when the location is known.

While it may be unlikely to know the exact position of the CT without GNSS, Fig. 9 highlights how performance can improve with some degree of location specificity. For example, the specific position of the CT may be unknown to the user, but knowing the general area such as the city, state, or country could still provide a notable performance boost.

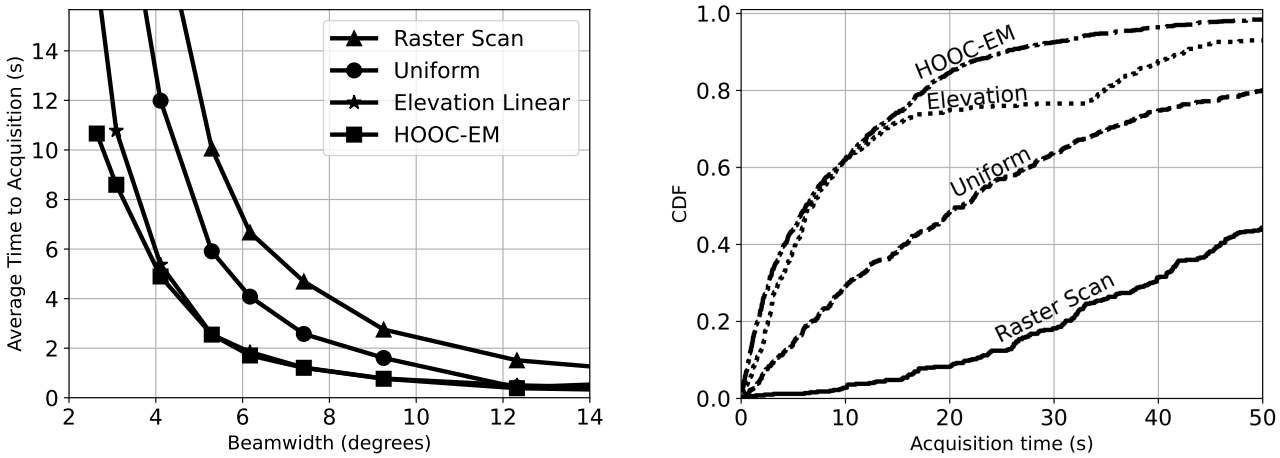

Figure 8: The average time to detection of the various beam sweeping methods (left) and their cumulative density functions (right) at a beamwidth of 2.64 degrees with $T_{\text{FAI}} = 15$ seconds.

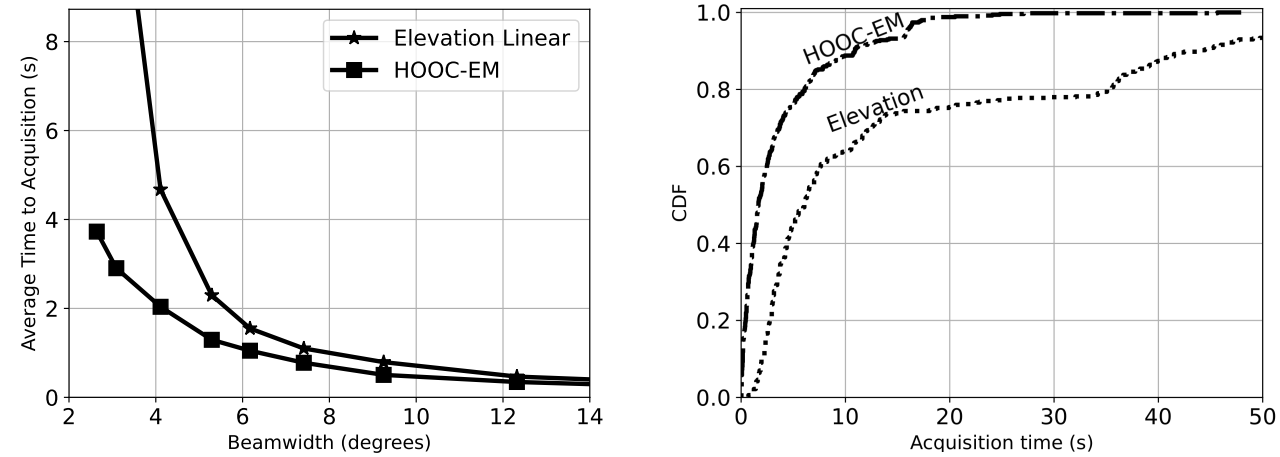

Figure 9: The average time to detection of the various beam sweeping methods (left) and their cumulative density functions (right) at a beamwidth of 2.64 degrees with $T_{\text{FAI}} = 15$ seconds and a known position.

V. CONCLUSIONS

This paper presented HOOC-EM, a novel method for fast CT beam sweeping in LEO mega-constellation networks. HOOC-EM consists of multiple algorithms: (1) partitioning the celestial sphere into hexagonal and pentagonal cells, (2) assigning probabilities to these cells based on satellite geometry, and (3) performing a maximum likelihood search of the partitioned celestial sphere that is dynamically updated according to satellite movement and the fixed assignment interval of the network. Simulations were conducted on an exemplar communications constellation modeled after the Amazon Kuiper-Ka constellation. HOOC-EM was evaluated against an elevation-first raster scan search, a uniform maximum-likelihood search, and an elevation-based maximum likelihood search.

The results showed that HOOC-EM outperformed the other methods at narrow beamwidths while performing comparably to the elevation-based search at wider beamwidths. Furthermore, the simulations also indicated that providing the CT with some information on its position may improve HOOC-EM search speeds. Analyses of the CDFs of the various search methods show that the HOOC-EM search has much shorter tails than the elevation-based search.

ACKNOWLEDGEMENTS

This work was supported by Amazon's Project Kuiper as an affiliate of the 6G@UT center within the Wireless Networking and Communications Group at The University of Texas at Austin.

REFERENCES

[3GPP, 2017] 3GPP (2017). Study on NR to support non-terrestrial networks. Tr 38.811, 3rd Generation Partnership Project (3GPP). Version 15.0.0.

[3GPP, 2023] 3GPP (2023). Solutions for NR to support non-terrestrial networks. Tr 38.821, 3rd Generation Partnership Project (3GPP). Version 16.0.0.

[Andrews et al., 2014] Andrews, J. G., Buzzi, S., Choi, W., Hanly, S. V., Lozano, A., Soong, A. C., and Zhang, J. C. (2014). What will 5G be? *IEEE Journal on selected areas in communications*, 32(6):1065–1082.

[Artiga and Vázquez, 2023] Artiga, X. and Vázquez, M. Á. (2023). Evaluation of new radio beam management framework for LEO satellites. In *2023 IEEE Conference on Standards for Communications and Networking (CSCN)*, pages 241–246. IEEE.

[Baykas et al., 2011] Baykas, T., Sum, C.-S., Lan, Z., Wang, J., Rahman, M. A., Harada, H., and Kato, S. (2011). IEEE 802.15. 3c: The first IEEE wireless standard for data rates over 1 Gb/s. *IEEE Communications Magazine*, 49(7):114–121.

[Blázquez-García et al., 2023] Blázquez-García, R., Cristallini, D., Ummenhofer, M., Seidel, V., Heckenbach, J., and O'Hagan, D. (2023). Experimental comparison of Starlink and OneWeb signals for passive radar. In *2023 IEEE Radar Conference (RadarConf23)*, pages 1–6.

[Chan, 1980] Chan, F. (1980). A quadrilateralized spherical cube earth data base. In *NASA. Goddard Space Flight Center Fifth Ann. Flight Mech.(Estimation Theory Symp.)*.

[Curtis, 2009] Curtis, H. D. (2009). *Orbital Mechanics for Engineering Students*. Elsevier, Burlington, MA, 2nd edition.

[Dimitrijević et al., 2016] Dimitrijević, A. M., Lambers, M., and Rančić, D. (2016). Comparison of spherical cube map projections used in planet-sized terrain rendering. *Facta Universitatis, Series: Mathematics and Informatics*, 31(2):259–297.

[Euler, 1758] Euler, L. (1758). Elementa doctrinae solidorum. *Novi commentarii academiae scientiarum Petropolitanae*, pages 109–140.

[Ghasempour et al., 2017] Ghasempour, Y., Da Silva, C. R., Cordeiro, C., and Knightly, E. W. (2017). IEEE 802.11 ay: Next-generation 60 GHz communication for 100 Gb/s Wi-Fi. *IEEE Communications Magazine*, 55(12):186–192.

[Heng et al., 2021] Heng, Y., Andrews, J. G., Mo, J., Va, V., Ali, A., Ng, B. L., and Zhang, J. C. (2021). Six key challenges for beam management in 5.5 G and 6G systems. *IEEE Communications Magazine*, 59(7):74–79.

[Humphreys et al., 2023] Humphreys, T. E., Iannucci, P. A., Komodromos, Z. M., and Graff, A. M. (2023). Signal structure of the Starlink Ku-band downlink. *IEEE Transactions on Aerospace and Electronic Systems*, pages 1–16.

[Iannucci and Humphreys, 2022] Iannucci, P. A. and Humphreys, T. E. (2022). Fused low-earth-orbit GNSS. *IEEE Transactions on Aerospace and Electronic Systems*, pages 1–1.

[Kim et al., 2020] Kim, J., Yun, M. Y., You, D., and Lee, M.-S. (2020). Beam management for 5G satellite systems based on NR. In *2020 International Conference on Information Networking (ICOIN)*, pages 32–34. IEEE.

[Komodromos et al., 2023] Komodromos, Z. M., Qin, W., and Humphreys, T. E. (2023). Signal simulator for Starlink Ku-Band downlink. In *Proceedings of the ION GNSS+ Meeting*, pages 2798–2812.

[Kummu and Varis, 2011] Kummu, M. and Varis, O. (2011). The world by latitudes: A global analysis of human population, development level and environment across the north–south axis over the past half century. *Applied geography*, 31(2):495–507.

[Kutkov, 2023] Kutkov, O. (2023). Connecting external gps antenna to the starlink terminal. https://olegkutkov.me/2023/11/07/connecting-external-gps-antenna-to-the-starlink-terminal/. Accessed: 2023-03-01.

[Maine et al., 1995] Maine, K., Devieux, C., and Swan, P. (1995). Overview of Iridium satellite network. In *WESCON/'95 Conference*, page 483. IEEE.

[Maral et al., 2020] Maral, G., Bousquet, M., and Sun, Z. (2020). *Satellite communications systems: systems, techniques and technology*. John Wiley & Sons.

[McCollum, 2001] McCollum, J. M. (2001). Honeycombing the icosahedron and icosahedroning the sphere[1]. In *Proceedings of the Second Annual Forest and Inventory Symposium: Salt Lake City, Utah, October 17-18, 2000*, volume 47, page 25. USDA Forest Service, Southern Research Station.

[Morales et al., 2019] Morales, J. J., Khalife, J., Cruz, U. S., and Kassas, Z. M. (2019). Orbit modeling for simultaneous tracking and navigation using LEO satellite signals. In *Proceedings of the 32nd International Technical Meeting of the Satellite Division of The Institute of Navigation (ION GNSS+ 2019)*, pages 2090–2099.

[Nitsche et al., 2014] Nitsche, T., Cordeiro, C., Flores, A. B., Knightly, E. W., Perahia, E., and Widmer, J. C. (2014). IEEE 802.11 ad: directional 60 GHz communication for multi-gigabit-per-second Wi-Fi. *IEEE Communications Magazine*, 52(12):132–141.

[Qin et al., 2023] Qin, W., Komodromos, Z. M., and Humphreys, T. E. (2023). An agile, portable antenna system for LEO megaconstellation-based PNT. In *Proceedings of the ION GNSS+ Meeting*.

[Rappaport et al., 2014] Rappaport, T. S., Heath Jr, R. W., Daniels, R. C., and Murdock, J. N. (2014). *Millimeter wave wireless communications*. Pearson Education.

[Rinaldi et al., 2020] Rinaldi, F., Määttänen, H.-L., Torsner, J., Pizzi, S., Andreev, S., Iera, A., Koucheryavy, Y., and Araniti, G. (2020). Broadcasting services over 5G NR enabled multi-beam non-terrestrial networks. *IEEE Transactions on Broadcasting*, 67(1):33–45.

[Robinson, 2002] Robinson, R. C. (2002). Perron frobenius theorem. *mij*, 10:0.

[Space Exploration Holdings, 2020] Space Exploration Holdings (2020). SpaceX Gen2 NGSO Satellite System, Attachment Waiver Requests. https://licensing.fcc.gov/myibfs/download.do?attachment_key=2378667. SAT-LOA-20200526-00055.

[Systems, 2019] Systems, K. (2019). Application for fixed satellite service by Kuiper Systems LLC. https://licensing.fcc.gov/myibfs/download.do?attachment_key=1773885. SAT-LOA-20190704-00057.

[Tegmark, 1996] Tegmark, M. (1996). An icosahedron-based method for pixelizing the celestial sphere. *The Astrophysical Journal*, 470(2):L81.

[Wei et al., 2023] Wei, W., Zheng, Z., Wang, Y., Su, Y., Wang, X., Liu, L., Wang, B., Sun, C., and Wang, D. (2023). Random access control and beam management scheme for the 5G NR based beam hopping LEO satellite communication systems. *Mobile Networks and Applications*, pages 1–12.

[Xue et al., 2024] Xue, Q., Ji, C., Ma, S., Guo, J., Xu, Y., Chen, Q., and Zhang, W. (2024). A survey of beam management for mmwave and THz communications towards 6G. *IEEE Communications Surveys & Tutorials*.